Universitat Autònoma de Barcelona
Facultat de Ciències
Departament de Física

Physics Final Degree Thesis

Fast ion populations during ion cyclotron resonance frequency heating in tokamaks

Thesis director:
Prof. Dr. Mervi Mantsinen

Author:
Gerard Castro

July 2021 Call

Abstract

The aim of this thesis is to improve the capabilities of a simplified modelling code PION, which models resonant ions in tokamak fusion reactors during 'Ion Cyclotron Resonance Frequency' (ICRF) heating. In particular, a simplified model is investigated in order to expand the pitch-angle-averaged velocity distribution function calculated by PION to a two-dimensional distribution function in velocity and pitch angle.

This improvement is of interest since it will allow new comparisons with fast ion measurements with various diagnostics for further validations of the code against experimental data. Experimental validation is of vital importance to increase our confidence in our simulations of new experiments with ICRF heating both in present devices and future devices such as ITER.

Keywords: fast ion populations, ICRF heating (ICRH), Fokker-Planck.

Acknowledgements

Despite the uncountable attractive phenomena which arise in nuclear physics, I started this journey mainly captivated by the idea of applying physics to an initiative that could lead to a better world.
However, if this thesis has been possible, it is thanks to Prof. Dr. Mervi Mantsinen, who has been my leading figure not only in the development of the project but also in my learning path. In addition, any of this would have neither been possible without the invaluable support and patience of Dr. Dani Gallart and Mr. Jordi Manyer.
Last but not least, I am also infinitely grateful to my family and friends for their everlasting affection and motivation. *A tots, moltes gràcies.*

Contents

Introduction **1**

1 Magnetic confinement fusion **3**
1.1 Ion's motion and plasma confinement device: tokamak 4
1.1.1 Particle orbits in a tokamak 6
1.2 Plasma heating methods: ICRF heating (ICRH) 7
1.2.1 Physics of ICRH 7
1.2.2 Damping mechanisms 8
1.2.3 Minority heating 8

2 Modeling of resonant ions **10**
2.1 Evolution of the distribution function 10
2.1.1 Small orbit widths 11
2.1.2 Pitch-angle averaged function 12

3 `PION` modeling and extension to a 2D FP distribution **14**
3.1 `PION` code modeling 14
3.2 Extension to a 2D FP distribution 15
3.2.1 Theoretical justification 15
3.2.2 $\Delta\xi$ calculation 17
3.2.3 $\mathcal{C}$ calculation 18
3.3 Numerical implementation 18

4 Numerical results **20**
4.1 Changing ICRH power 23
4.2 Changing ICRH resonance position 24

5 Conclusions **26**

List of Figures

1.1 Schemes of both the geometry of a tokamak and its characteristic flux surfaces. 5
1.2 Sketches of the possible ions orbits in a tokamak and of the resonance layer. . 6

4.1 Plots of the exponential Ansatz in pitch-angle vs. energy plane (η, E). 21
4.2 Plots of the midplane pitch-angle ξ as function of the poloidal angle θ. 21
4.3 Plots of the $2D$ η-integrated distribution function f_0 in (R, Z) coordinates. . . 22
4.4 Plots of the $2D$ η-integrated distribution function f_0 in (R, Z) coordinates for different ICRH power. 23
4.5 Plots of the $2D$ η-integrated distribution function f_0 in (R, Z) coordinates for different ICRH frequency. 25

Introduction

Preface

Not only do the huge impact fossil fuels based energies represent on the environment, but also its finiteness in a growing society which increasingly depends on energy are the main driving forces in the exploration of alternative and robust sources of clean energy.

Yet, fusion energy stands as one of the most promising candidates; specifically, when achieved by confining highly heated plasma with strong magnetic fields in a device known as *tokamak*.

Fusion energy is, unlike its fission counterpart, virtually unlimited (since its fuel is mainly light atoms, as hydrogen and its isotopes), safe (as it cannot occur uncontrollable chain reactions) and the products arisen from the nuclear reactions are harmless.

Being able to reach high temperatures ($\sim 10^6$ K) is essential in order to achieve the maximum fusion cross section; namely, the number of fusion reactions. With that intention, many different strategies have been developed to achieve such great temperatures.

This thesis deals with the heating of a fusion plasma in a tokamak using electromagnetic waves (EM) in the range of radio frequency, close to the ion cyclotron resonance frequency. This is also known as 'Ion Cyclotron Resonance Frequency Heating' (ICRH or ICRF heating).

More specifically, this work tackles theoretically and numerically the modeling of resonant ions in tokamak plasmas during ICRF heating in terms of its corresponding distribution function. Note that being able to compute the distribution function of resonant ions is necessary to describe their behavior and interaction with the plasma.

Objectives and motivation

The aim of this thesis is to improve the capabilities of a simplified ICRH modeling code `PION`[30], which models resonant ions in tokamak fusion reactors during ICRH. In particular, a simplified model is investigated in order to expand the pitch-angle-averaged velocity distribution function calculated by `PION` to a two-dimensional $2D$ distribution function in velocity and pitch angle.

This improvement is of interest since it will allow new comparisons with fast ion measurements with various diagnostics for further validations of the code against experimental data.

Experimental validation is of vital importance to increase our confidence in our simulations of new experiments with ICRF heating both in present devices and future devices such as ITER.

Specifically, the main guidelines with which this work is developed list as follows:

1. To provide a brief introduction of the main physical aspects of confined fusion and ICRH.
2. To carry out a thorough review of the most important models of ICRH resonant ions, yielding to the $1D$ function in velocity that is currently being used in the `PION` code.
3. **To present a $2D$ expansion of the distribution function as means of adding a pitch dependency to the current $1D$ `PION` function, improving its capabilities.**
4. **To obtain some figures and numerical results using the presented distribution function, discussing and comparing to the experimental expected outcome.**

Regarding the structure, each previous item is covered by its corresponding chapter (with the same enumeration), while a summary of the results is given in chapter 5.

Chapter 1

Magnetic confinement fusion

For nuclear fusion to be a viable energy source, the output (total fusion) power must be higher than the input power (heating power): which is a quality factor Q higher than 1, $Q > 1$.

In particular, the corresponding main reaction has to be exothermic. This means the nuclear reaction delivers energy in form of kinetic energy, which is the result from the mass difference between the initial nuclei (that fuse) and the final nucleus. This kind of processes only occurs for elements with an atomic number below $Z < 26$.

So far, nuclear fusion has been mainly addressed in terms of several reactions involving hydrogen H and its isotopes (deuterium D and tritium T) and helium He, being of particular importance the following reaction[1]:

$$D + D \rightarrow \begin{cases} T\ (1.01\ \mathrm{MeV}) + p\ (3.02\ \mathrm{MeV}) \\ {}^{3}\mathrm{He}\ (0.82\ \mathrm{MeV}) + n\ (2.45\ \mathrm{MeV}) \end{cases} \tag{1.1}$$

The numbers in parenthesis stand for the kinetic energy of the end product particles assuming that the initial nuclei have zero kinetic energy. So far the D-D reaction (1.1) has been the main process studied and used, e.g in the Joint European Torus (JET[31]) and AUG[32] tokamaks.

The preference for a reaction is in general justified not only in terms of the amount of energy it delivers, but also because it presents a high cross-section[1]. For instance, $\sigma_{DD} \sim 10^{-29}\ \mathrm{m}^2$ for an energy around $100\ \mathrm{keV}$, in the (1.1) case.

These nuclear processes clearly do not occur spontaneously in normal conditions, but instead their energy thresholds correspond to huge amounts of ion temperature and velocity. For instance, the peak of σ_{DT} corresponds to a temperature of $1.5{\cdot}10^{8}\ \mathrm{K}$. At such temperature, matter becomes fully ionized constituting a 'gas' of free electrons and nuclei known as plasma.

Thus, in order to use nuclear fusion as a clean energy source, two main technical difficulties have to be addressed:

- How to contain and control this 'hot' plasma.
- How to heat this plasma to achieve temperatures of $T \sim 10^{8}\ \mathrm{K}$.

[1] It is well-known that, for nuclear processes, the higher the cross-section σ is, the more possibilities exist for the reaction to occur.

The following subsections are devoted, respectively, to review some of the most important techniques to answer these challenges.

1.1 Ion's motion and plasma confinement device: tokamak

As mentioned above, the state of matter in which fusions occur is plasma, which can be thought as an ionized gas that fulfils certain conditions.

Even though this plasma can be controlled by means of other techniques (see, for instance, inertial confinement fusion ICF[2]), in this thesis it will be discussed the magnetic confinement fusion. This technique achieves the plasma confinement by applying a magnetic field $\mathbf{B}$.

By Lorentz force, ions and electrons spin around the magnetic field lines, as shown in Figure 1.1a, being their trajectory $\mathbf{r}$ given by cylindrical coordinates $\mathbf{r} = \mathbf{z} + \mathbf{r}_\perp$, where:

$$\mathbf{r}_\perp = \frac{v_\perp}{\omega_c}\left[\cos\left(\omega_c t + \phi\right)\hat{i} + \sin\left(\omega_c t + \phi\right)\hat{j}\right], \quad \mathbf{z} = \left(v_\parallel t\right)\hat{k}$$

Where $v_\parallel$ ($v_\perp$) is the parallel (perpendicular) velocity to the magnetic field such that $v_\perp = |\mathbf{r}_\perp|\omega_c$, ϕ is an arbitrary phase angle and ω_c the cyclotron frequency defined as $\omega_c = \frac{ZeB}{Am_p}$.

Currently, the so-called *tokamak* is the most promising device for plasma magnetic confinement since it presents better performance than other choices, *e.g.* the *stellarator*. The tokamak is a symmetric toroidal fusion device which is composed by an array of toroidal magnets that produces a constant magnetic toroidal field $\mathbf{B}_\phi$ inside the vacuum vessel and a central solenoid that induces a plasma current I_p. As represented in Figure 1.1a, this current produces in turn a poloidal magnetic field $\mathbf{B}_\theta$ (forming a helical magnetic field line), such that $\mathbf{B}_\theta \ll \mathbf{B}_\phi$.

With this magnetic field shape, the plasma can be confined and the radial equilibrium kept. Besides, since toroidal magnets are closer to the centre of the torus than to the outer edge, the toroidal magnetic field decreases as $B_\phi \propto \frac{1}{R}$, being R the radial distance from the torus axis.

Moreover, the tokamak does not present exactly circular poloidal sections, but they are 'D-shaped' (this will be clearly seen in Figures 4.3, 4.4, 4.5). This explains why toroidal coordinates are not the only ones used to describe the physics of this device, but instead (R, Z) for each poloidal section. As schemed in Figure 1.1a, R indicates the projection perpendicular to the vertical axis ($\perp \mathbf{B}$) of the distance from the center of the tokamak; while Z gives the vertical component of this distance. In this geometry, the horizontal line $Z = 0$ is called midplane; while the values such that $R > R_0$, being R_0 evaluated at the center of the midplane, correspond to the so-called 'low field side' (LFS) of the tokamak. Contrarily, $R < R_0$ belong to the 'high field side' (HFS).

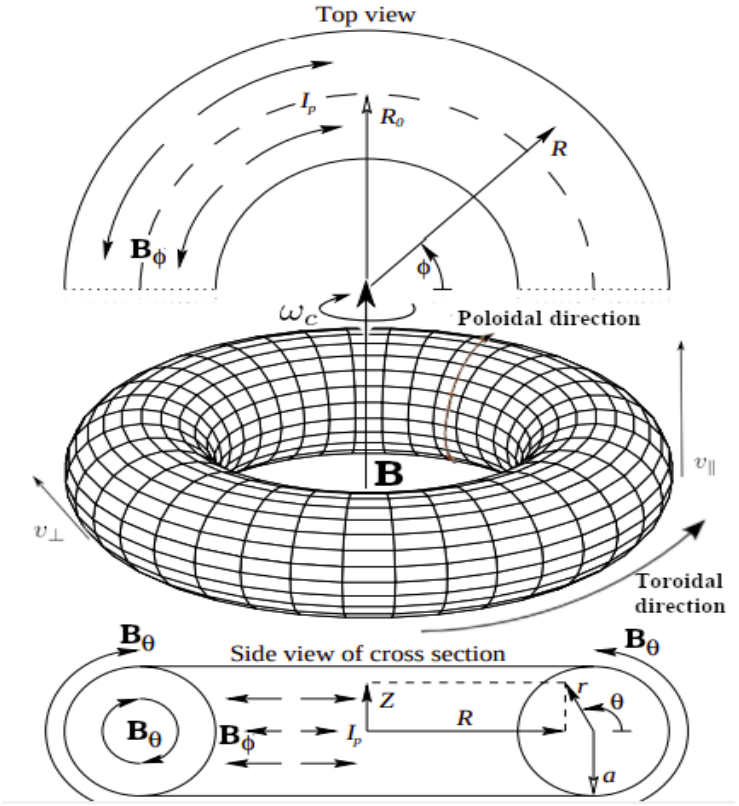

(a) Scheme of the tokamak geometry and the main magnitudes associated with the ions' trajectory. This figure is a modification of the original image presented at page 13 of Hedin[20].

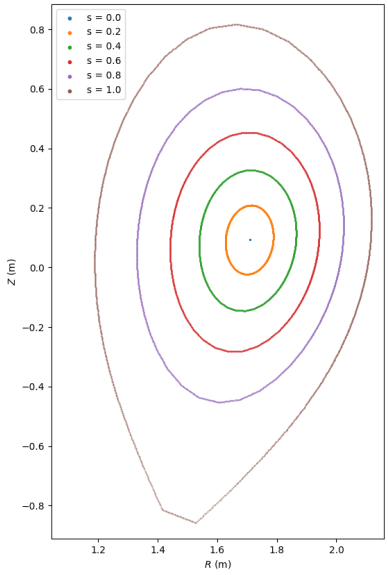

(b) Poloidal flux surfaces in a tokamak labeled with their corresponding value of $0 \leq s \leq 1$, for $t \approx 3$ of shot 38017 in a experiment performed in the AUG tokamak.

Figure 1.1: Schemes of both the geometry of a tokamak, (a), and its characteristic flux surfaces, (b).

Furthermore, when studying ion's movement and its magnitudes, it is customary to define the so-called poloidal flux surface label s. Actually, s is the positive square root of the normalized poloidal flux function ψ so, as there is a bijection between s and ψ, both magnitudes can be treated equivalently: $s \leftrightarrow \psi$.

The contour lines of s (or ψ), that is the set of R, Z for which $s(R, Z)$ has a fixed certain value, represent the 'flux surfaces' in which the pressure is constant[6] or, equivalently, have same direction than $\mathbf{B}_\theta$ and the poloidal magnetic flux is the same (Figure 11.8 of Freidberg[6] gives a clear explicit visualization). In particular, this contour lines define different closed lines in the poloidal section of a tokamak, see Figure 1.1b, they are useful for the ion's modeling. Specifically, s or ψ are commonly set as parameters to describe the physical domain in real space. We will refer to a certain poloidal flux surface unambiguously by its label s.

1.1.1 Particle orbits in a tokamak

The description of ions motion must have into account the type of orbits they can follow, as well. There are many types of particle orbits in a tokamak. The two main types are passing and trapped orbits as shown in Figure 1.2a.

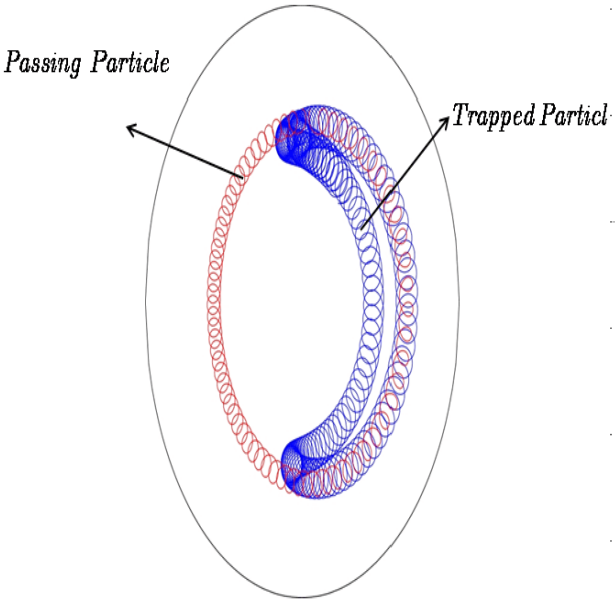

(a) Sketch of the poloidal orbits of passing and trapped particles. This figure was taken from Dini et al.[4].

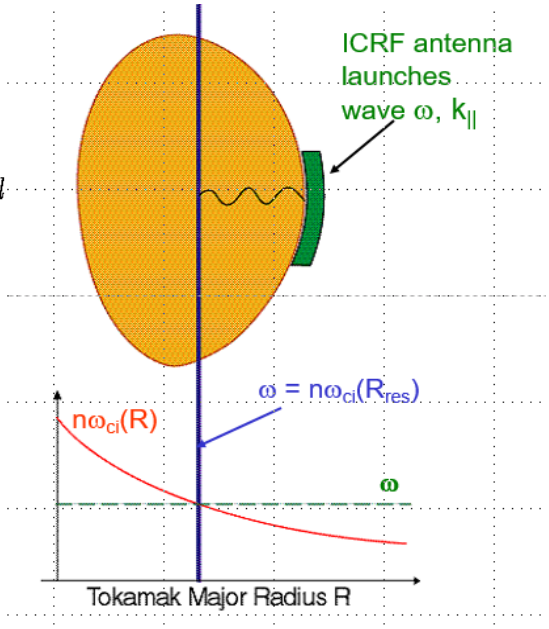

(b) Sketch of the resonance layer (blue line) during ICRH. The turning points of the trapped ions orbits are found at $R = R_{\text{res}}$. This R_{res} is such that the ICRF waves (launched from the LFS) match their frequency ω according to the resonance condition (1.2) for a given cyclotron frequency $\omega_c(R_{\text{res}})$ and $k_\parallel v_\parallel = 0$.

Figure 1.2: Sketches of the possible ions orbits (a) in a tokamak and the resonance layer (b).

The particle orbits can be characterized by the constants of particle motion, or so called

invariants. Such invariants include for instance, quantities proportional to the energy $E = m\frac{v^2}{2}$ and the magnetic moment μ, as seen in section 2.1.

The magnetic moment is a key quantity specially in ICRH, the heating method tackled in this work and reviewed in section 1.2. Because of the conservation of magnetic moment μ, in ICRH we can have much more **trapped ions** in tokamaks. In particular, **ICRH tends to increase** the perpendicular velocity and, when doing so, the **number of trapped particles** in the distribution function. These particles behave similarly to passing particles with the exception that their poloidal orbit is not an 'ellipse' anymore, but a kind of **'banana' shaped** orbit, as shown in Figure 1.2a. More specifically, these kind of orbits have their turning points along the resonance layer, that is located at a given $\mathbf{B}$, located vertically in the poloidal plane as shown with a blue line in Figure 1.2b. It is in these turning points that the **parallel velocity becomes zero** and then the particles goes back traversing this banana orbit.

Thus, and as reviewed in section 1.2, ICRF heating not only increases the number of trapped ions but also positions of the turning points of the trapped ions vanishes along the resonance layer.

1.2 Plasma heating methods: ICRF heating (ICRH)

Plasma must achieve high temperatures so that the reactions cross-sections σ are high enough for the processes to occur; therefore, plasma heating is necessary to carry out nuclear fusion.

Apart from just Ohmic heating, *i.e.* heating due to the passage of electrical current through it, there are auxiliary heating methods to heat the plasma. For instance, the so-called neutral beam injection (NBI) and radio-frequency (RF) heating are viable mechanisms currently used to further increase plasma temperature.

In this thesis, NBI heating will not be discussed, instead we will address RF heating. This method consists of launching EM waves with antennas placed inside the vacuum vessel; then, the waves are eventually damped by ions and electrons effectively rising the plasma temperature. RF heating can be used to heat electrons (ECRH), ions (ICRH), or to produce non inductive currents in the plasma (LHCD), depending on the frequency of the wave ω (for more details on NBI see [5], while about RF heating see [6], [7]).

1.2.1 Physics of ICRH

The ion energy absorption is strictly related to the ICRF wave electric field $\mathbf{E}$ which, in turn, depends on their propagation in the plasma. Thus, it is a coupled problem and, in order to model and control ion power deposition, the ICRF wave propagation must be also be taken into account.

In particular, while the wave propagation is governed by Maxwell's equations (taking into account the modifications due to the resonant ions as they are damped by wave), the plasma is modeled according to the so-called cold plasma model[1], [23].

However, a complete analysis of this coupled problem goes much beyond the goals of this thesis, which focuses on the characteristics of these resonant ion populations instead.

1.2.2 Damping mechanisms

ICRF waves can heat ions but also electrons and they can even produce non-inductive currents to the plasma. Regarding ions power deposition alone, their wave damping is governed by a resonance condition in their equation of motion, affected by $\mathbf{E}$. This condition is met when the Doppler-shifted wave frequency $\omega - v_\parallel k_\parallel$ matches the ion cyclotron frequency ω_c or its harmonic n (being $n = 1$ the fundamental)

$$\omega = k_\parallel v_\parallel + n\omega_c \ , \quad n = 1, 2, \dots \tag{1.2}$$

Where $k_\parallel$ is the component of the wave number parallel to the background magnetic field. Besides, even though $v_\perp$ does not determine 'when' the damping occurs, it determines the strength of the absorption. Concretely, the kick in energy for $v_\perp$ that an ion experiences when passing through a resonance region scales as[15]

$$\Delta v_\perp \propto \left[E_+ J_{n-1}\left(\frac{k_\perp v_\perp}{\omega_c}\right) + E_- J_{n+1}\left(\frac{k_\perp v_\perp}{\omega_c}\right) \right] \ , \tag{1.3}$$

where[9] $E_\pm := \frac{1}{\sqrt{2}}\left(E_x \pm iE_y\right)$ is the left (right) circularly polarized wave, n is the cyclotron harmonic and J_n is the n-th Bessel function of the first kind.

The analysis of wave damping is much more complex in reality. Although this work does not tackle these aspects with detail, it is worth noting that ICRF wave frequency not only characterize the strength of the damping, but also the position of the ion resonance and the features of the resonant ions populations. Namely, ICRF heating tends to increase the number of trapped particle orbits, with their tips at the ICRF resonance layer.

In particular, during ICRF heating, the energy of passing particles in the perpendicular velocity direction is being increased until at some point these particles become trapped. The banana shaped orbits of this trapped particles (see section 1.1) have their turning points along the resonance layer, which is a vertical layer located at $R = R_{\text{res}}$. This resonance position R_{res} is such that, for a given ω_c and $\mathbf{B}$, ω satisfies (1.2).

This can be seen schematically in Figure 1.2b and it will also justify the form of the Ansatz proposed at section 3.2.1 (and the way to extend it in the ξ variable based on the conservation of magnetic moment).

1.2.3 Minority heating

Minority heating is commonly applied for fundamental ion cyclotron resonance (whenever the ICRF wave frequency ω equals the ion i cyclotron frequency $\omega_{c_i} =: \omega_c$). Such technique is based in adding a small amount, normally a few percent, of an extra ion species j with higher ion cyclotron frequency ω_{c_j} than the frequency ω_c of the majority ion species i.

The purpose of this is to ensure ion absorption to effectively raise temperature of plasma. Since the actual fraction of power absorbed depends upon the ratio of $\frac{E_+}{E_-}$, the method ensures this fraction does not vanish. In particular, it can be seen[1], [2] that according to the plasma cold model that:

$$\frac{E_+}{E_-} = \frac{\omega_c - \omega}{\omega + \omega_c} \ , \tag{1.4}$$

which clearly implies that, for fundamental ICRF resonance $\omega = \omega_c$, the wave is entirely right polarized $E_+ = 0$ just at the point where a left polarized wave is needed for damping.

Therefore, adding a minority ion species j (such as hydrogen H in D plasma) prevents the numerator of (1.4) from vanishing and, thus, the wave presents the necessary left polarization.

This will be the case of the experimental data used in section 4, where H minority heating in D plasma is addressed.

Chapter 2

Modeling of resonant ions

With the purpose of completely characterizing resonant ions, plasma must be well defined and described. It is both analytically and numerically unfeasible to solve the $3\ \mathrm{N}$ equations of motion (assuming the plasma contains N ions): $\mathbf{F}_i = m_i \mathbf{a}_i$, where the force acting on the i-th particle $\mathbf{F}_i$ is determined by the influence of all the other particles.

Instead it will be dealt on a macroscopic scale, in terms of the distribution function $f(\mathbf{r}, \mathbf{v}, t)$ which retrieves the density of particles in a time dependent-$6D$ phase space, such that $\int d\mathbf{r} d\mathbf{v} f = N$.

However, we will consider the case in which the distribution function is normalized $\int d\mathbf{r} d\mathbf{v} f = 1$, and, thus, $f d\mathbf{r} d\mathbf{v}$ represents the probability for a particle to be in the volume $d\mathbf{r} d\mathbf{v}$.

The behavior and evolution of this plasma as function of time is described by the Boltzmann equation

$$\frac{\partial f(\mathbf{r}, \mathbf{v})}{\partial t} + \mathbf{v} \cdot \nabla f(\mathbf{r}, \mathbf{v}) - \frac{q}{m}(\mathbf{E} + \mathbf{v} \times \mathbf{B}) \cdot \frac{\partial f}{\partial \mathbf{v}} = \left.\frac{\partial f}{\partial t}\right|_{\mathrm{C}} , \tag{2.1}$$

where q, m are the electric charge and the mass of the described ion species, respectively, while the right hand side is a non-trivial collision operator.

Notice that the left hand side is straight-forwardly obtained by developing the $f(\mathbf{r}, \mathbf{v}, t)$ differential: $df = \frac{\partial f}{\partial t} dt + \nabla f \cdot d\mathbf{r} + \frac{\partial f}{\partial \mathbf{v}} \cdot d\mathbf{v} = \frac{\partial f}{\partial t} dt + \nabla f \cdot \mathbf{v} dt + \frac{1}{m} \frac{\partial f}{\partial \mathbf{v}} \cdot \mathbf{F} dt$; since $\mathbf{v} = \frac{d\mathbf{r}}{dt}$ and $dv = \frac{\mathbf{F}}{m} dt$, where $\mathbf{F}$ is the external force field acting on the particles in the plasma.

Besides, while the $\frac{q}{m}(\mathbf{E} + \mathbf{v} \times \mathbf{B}) \cdot \frac{\partial f}{\partial \mathbf{v}}$ term can be clearly identified as the 'force' term, the $\mathbf{v} \cdot \nabla f(\mathbf{r}, \mathbf{v})$ can be thought as a 'diffusion' term.

2.1 Evolution of the distribution function

If the force from the wave field, as well as the 'diffusion' term, of (2.1) are written as operators on the distribution function, then an orbit-averaged Fokker-Planck equation can describe[17] f.In particular, f is the solution of

$$\frac{\partial f(\mathbf{r}, \mathbf{v})}{\partial t} = \langle C\left[f(\mathbf{r}, \mathbf{v})\right] \rangle + \langle Q\left[f(\mathbf{r}, \mathbf{v})\right] \rangle , \tag{2.2}$$

where C is the so-called collision operator and Q is the quasi-linear RF operator for wave particle interaction. This orbit-average is defined as

$$\langle \cdots \rangle = \int\int\int (\cdots)\, d\theta_1 d\theta_2 d\theta_3 \ , \tag{2.3}$$

where θ_1, θ_2 and θ_3 are the angles which describe respectively, and usually, the position of a particle in the so-called Larmor rotation, the poloidal position along the guiding center orbit and the toroidal position of the 'banana'[1] center, respectively.

Reducing, by these 3 angles, the t-dependent $6D$ phase space leaves 3 free variables to fully characterize the motion of a particle. These are the motion invariants, see section 1.1, and they are usually chosen as[16]:

$$\tilde{E} = \frac{v^2}{2}, \quad \Lambda = \frac{B_0 v_\perp^2}{B v^2} \equiv \frac{\mu B_0}{E}, \quad \tilde{P}_\phi = R v_\parallel + \frac{q}{m}\psi \ ,$$

being B_0 the magnetic field at the axis and ψ is the poloidal flux function and μ the magnetic moment. With this choice of variables, the quasi-linear operator is written as[15] $\langle Q(f) \rangle = \sum_N L_N \left(D_{RF}^N L_N f \right)$, where L_N and the diffusion coefficient D_{RF}^N are:

$$\begin{cases} L_N = & \frac{\partial}{\partial E} + \frac{n\omega_0 - \Lambda\omega}{\omega E}\frac{\partial}{\partial \Lambda} + \frac{N}{\omega}\frac{\partial}{\partial P_\phi} \ , \\ D_{RF}^N = & \frac{1}{4\omega^2}\sum_R \frac{(Ze)^2}{|n\dot{\omega}_{cR}|} v_{\perp R}^2 \left[E_+ J_{n-1}\left(\frac{k_\perp v_{\perp R}}{\omega_{cn}}\right) + E_- J_{n+1}\left(\frac{k_\perp v_{\perp R}}{\omega_{cR}}\right)\right]^2 \ . \end{cases}$$

Where J_{n-1} is the $n-1$-th Bessel function, being n the harmonic number (1.2), and the subscript R refers to a quantity evaluated at a resonance. More details on the calculation of $\langle C\,[f] \rangle$ are given in [15].

2.1.1 Small orbit widths

For small orbit widths, *i.e.* when particles tend to stay in the same flux surface s, an analysis of the solution of (2.2) can be made just in terms of two variables (v, η) for a **given magnetic surface** s (which will be set as fixed parameter, as the time t): these 2 variables can be the velocity v and the cosine of the pitch-angle $\eta := \frac{v_\parallel}{v}$. Equivalently, it can also be done in terms of $\left(v_\perp, v_\parallel\right)$. This analysis was initiated by Stix[9] and later on generalized by Anderson et al.[10] to include ICRH heating in higher harmonics and higher order effects.

This situation is complicated to formalize by the fact the distribution function obtained as solution of (2.2) consists of **an almost Maxwellian low-energy bulk part plus a strongly anisotropic energy tail for high velocities/energies**. This is because the collision frequency decreases with energy, while during intense heating the absorption preferentially heats the ions in the perpendicular direction.

Thus, even though (v, η) are the natural variables for the collision operator, they are not very appropriate when analyzing the high energy tail. It happens conversely to $(v_\perp, v_\parallel)$. In consequence, and reminding $v = \sqrt{v_\perp^2 + v_\parallel^2}$, $\eta = \frac{v_\parallel}{v}$, the explicit forms of the collision and RF-diffusion operators are given below in terms of (v, η) and $(v_\perp, v_\parallel)$, respectively. If just

[1] This term refers to the shape of the orbits for a flux surface.

the leading order for $\langle Q[f]\rangle$ is taken, and thus dependencies on the J_{n+1} term neglected, we obtain:

$$\begin{cases} \langle C[f]\rangle & = -\frac{1}{v^2}\frac{\partial}{\partial v}\left(v^2\alpha f\right) + \frac{1}{2v^2}\frac{\partial^2}{\partial v^2}\left(v^2\beta f\right) + \frac{1}{4v^2}\frac{\partial}{\partial \eta}\left(1-\eta^2\right)\frac{\partial}{\partial \eta}(\gamma f)\ , \\ \langle Q[f]\rangle & = \frac{K_n}{v_\perp}\frac{\partial}{\partial v_\perp}\left(v_\perp J_{n-1}^2\left(\frac{k_\perp v_\perp}{\omega_c}\right)\frac{\partial f}{\partial v_\perp}\right)\ . \end{cases}$$

where α, β, γ are the so-called Spitzer's Coulomb diffusion coefficients[3]; K_n is a constant proportional[10] to $|E_+|^2$.

As most of the particles can be expected to be almost isotropic (with only a small elongation in the direction of the perpendicular velocity coordinate), a natural viewpoint from which to solve (2.2) with the former operators, is to express $f, \langle C(f)\rangle, \langle Q(f)\rangle$ in the variables (v, η) and to expand $f(v,\eta)$ in terms of Legendre polynomials $P_k(\eta)$, such that[10]:

$$f(v,\eta) = \sum_{k=0}^{\infty} A_{2k}(v)P_{2k}(\eta)\ . \tag{2.4}$$

It can be seen P_k are the eigenfunctions of the collisional operator with associated λ_n eigenvalue, while A_{2k} is the solution of

$$\begin{aligned} \frac{\partial A_{2k}}{\partial t} = &-\frac{1}{v^2}\frac{d}{dv}\left[\alpha v^2 A_{2k} + \frac{1}{2}\frac{d}{dv}\left(\beta v^2 A_{2k}\right)\right] + \frac{\lambda_{2k}\gamma}{4v^2}A_{2k} \\ &+ \frac{\int_\eta P_{2k}(\eta) Q\left(\sum_{k=0}^{+\infty} A_{2k}P_{2k}(\eta)\right)d\eta}{\int_\eta P_{2k}^2(\eta)d\eta}\ . \end{aligned}$$

2.1.2 Pitch-angle averaged function

Even though (2.4) is already an approximation for small orbit widths which just depends on two variables (and s, t as parameters), its numerical computation can represent significant amounts of computing time. In order to reduce it, the one-dimensional pitch-angle-averaged Fokker-Planck can be solved instead. That is, an equivalent (2.4) solution averaged for all the values of η taken along a given magnetic surface s (for a certain time).

Actually, it turns out that this pitch-angle averaged distribution can describe well f through the solution proposed by Anderson et al.[8], [10]

$$\frac{\partial f}{\partial t} = \frac{1}{v^2}\frac{\partial}{\partial v}\left[-\alpha v^2 f + \frac{1}{2}\frac{\partial}{\partial v}\left(\beta v^2 f\right)\right] + \frac{1}{v^2}\frac{\partial}{\partial v}\left[v^2 D_{\mathrm{RF}}\frac{\partial f}{\partial v}\right]\ , \tag{2.5}$$

where the first term on the right-hand side is the pitch-angle averaged version of the collisional operator $\langle C\left[f\right]\rangle$, while the second term is the wave-particle interaction RF counterpart $\langle Q\left[f\right]\rangle$. The diffusion coefficient D_{RF} is

$$D_{\mathrm{RF}} = \frac{1}{2}\int_{-1}^{1} K_n \left| J_{n-1}\left(\frac{k_\perp v}{\omega_c}\sqrt{1-\eta^2}\right) + \frac{\mathrm{E}_-}{\mathrm{E}_+}J_{n+1}\left(\frac{k_\perp v}{\omega_c}\sqrt{1-\eta^2}\right)\right|^2 d\eta\ .$$

Keeping section 2.1.1 notation for K_n, α, β. Henceforward, this **solution of** (2.5) **will be written as** F. According to Anderson et al.(1987)[13], when comparing isotropic moments calculated with this model of the pitch-angle averaged distribution and the two dimensional 'BAFIC' code[11], good agreement has been found.

Despite its reasonable computing time of (2.5) and the accuracy of the approximation of $f(t, \mathbf{r}, \mathbf{v})$ by $F(v; s, t)$, in section 3 it is presented an extension of $F(v; s, t)$ to a 2D f_0 distribution function which recovers the pitch dependency, implicitly accounts for the poloidal angle θ and is built directly from F.

Chapter 3

PION modeling and extension to a 2D FP distribution

A complete description of the plasma's resonant ions is essential to compute the power deposition from EM waves to the ions in ICRH. Furthermore, at the same time, notice the description of the ions must be accurate enough since the variation of ICRH parameters implies great different consequences on the distribution function[20]. Namely, the wave absorption can provide ion and electron heating, but also non-inductive current drive, to give rise to plasma rotation... all depending on the ICRF frequency, concentration of the resonating species or toroidal wave spectrum, for instance.

Moreover, variations of the distribution function cause variations of the propagation of the wave; therefore, the profile of deposited power will in its turn affect the distribution function. Thus, it is a 'coupled' problem which requires self-consistent calculations of the wave field and distribution function in order to model ICRH heating.

Currently, the ITER experiment relies on the so-called 'Integrated Modelling & Analysis Suite' (IMAS[37]), a code framework which supports both plasma operation and its research activities. In particular, integrated in IMAS, it can be found the PION code for ICRF heating which, exactly, computes the EM wave power absorption in the ICRF range and the distribution function of the ions resonant with these waves in a self-consistent way.

Henceforth, the PION code and its outputs will act as numerical data from which the $2D$ extension of (2.5) distribution function $F(v; s, t)$ is built. Below, section 3.1 is devoted to a brief review of the PION code modeling details; while in subsection 3.2 the extension of the current distribution function is presented and discussed using PION simulated data.

3.1 PION code modeling

Currently PION is based on simplified models, which makes it 'fast' to use by an integrated modelling framework such as IMAS. For each time step, PION firstly computes the power absorbed and, using this information is then calculated the distribution function, which will be used to compute the absorption power at the beginning of the next time step.

Even though an analysis of PION code modeling is much beyond the goals of this thesis; some additional details are provided below. For more information, see section 3 of Gallart[1].

- The power deposition model was developed by Hellsten and Villard[24] and it was partially obtained by analyzing results from the full wave code LION[25], [26]. The power deposition is currently computed by Fourier decomposing the launched wave in the toroidal direction and calculating the power deposition for each toroidal mode number[24], [27].
- The **distribution function** corresponds to[1] **the solution** F **of expression** (2.5).
- Finally, in order to make both two former computations self-consistent, PION uses a model developed by Eriksson and Hellsten[28] for the dielectric tensor, that is the wave propagation/interaction with plasma essentially.

Although the code is based on the former simplified models, its validity has been checked and the code used in the IMAS[30]. Specifically, PION has been extensively used and benchmarked against different tokamaks, such as[1]: JET[31], AUG[32], Tore Supra[33], DIII-D[34], ITER[35] and DEMO[36].

Despite the versatility of a $1D$ description, whose use is mainly justified in terms of low computational times, the current distribution function does not allow to study the resonant ions density for different pitch or different poloidal positions. In the following subsection, a $2D$ extension for the former FP distribution is presented for a more detailed description.

3.2 Extension to a 2D FP distribution

3.2.1 Theoretical justification

In section 2 we discussed how the general $6D$ distribution function, where time is thought as parameter, could be approximated by a $3D$ orbit-averaged expression for each flux surface s we considered, also thought as parameter. The latter was actually $2D$ for small-orbit widths and, if the pitch-angle η average was considered, then the general expression could be approximated by the $1D$ (2.5) solution (for each flux surface s and time t): $F(v; s, t)$.

However, we would like to extend the former $1D$ $F(v; s, t)$ function to extend it to a $2D$ phase space dependency. One approach could be followed, for instance, could be to solve (2.4); nevertheless, in order to keep low computation times, it would be preferable to expand the dependency by using the already determined $1D$ distribution.

With that purpose, we consider the leading term f_0 of the distribution function f after a standard bounce averaging procedure. A "bounce-average" over the 'bounce' or toroidal transit motion of the particle reduces[38] the FP equation to be essentially $2D$ in the phase-space for each flux surface s (that is, considering s as a parameter).

[1] Actually, the solved expression is identical with a slight exception: a concrete S term in the right hand side to take into account ICRH+NBI (Neural Beam Injection) synergy and which is especially important in those experiments where neutral beams are in resonance with the wave[1].

This procedure is appropriate in cases where the bounce/transit time of the particles, τ_b, is shorter as compared to the collision time τ_c, i.e. $\tau_b \ll \tau_c$. See, also, [40] for more information. As remarked by Yau[38], this belongs to the current case since, not only in the present generation of larger tokamak experimental devices often operate with most of the plasma in this low-collisionality regime, but also non-Maxwellian particles generated by auxiliary heating and current drive usually are in the low-collisionality regime.

The variables on which f_0 depends can be chosen as $(v, \xi; s, t)$ - being s, t parameters -, where $\xi := \frac{v_{\parallel 0}}{v}$ is the pitch angle of a particle orbit in the outer midplane ($Z = 0$ in RZ plane). It can be seen[39] $\frac{\partial f_0}{\partial \theta} = 0$ and, thus, f_0 does not explicitly depend on θ. However, an implicit dependence is found through ξ, since by conservation of magnetic momentum it is held

$$\frac{1-\eta^2}{B(s,\theta;t)} = \frac{1-\xi^2}{B_0(s;t)} \ , \tag{3.1}$$

where $\eta := \frac{v_\parallel}{v}$ is the particle pitch angle, $B(s, \theta; t)$ is the toroidal magnetic field (written as B_ϕ in section 1) evaluated in a flux surface s for a poloidal position θ, while $B_0(s; t) := B(s, 0; t)$ is the same field evaluated at midplane $\theta = 0$.

Actually, the conservation of magnetic moment μ, an invariant of motion for passing particles (section 1.1), not only provides a dependency of (η, θ) through ξ but also it **implies the existence of trapped particles** with banana orbits.

Moreover, it **provides a clear way** to expand $F(v; s, t)$ to a $2D$ distribution function $f_0(v, \xi; s, t)$ in terms of an 'Ansatz' of the form:

$$\text{Ansatz} = \left[\exp\left(-\left(\frac{\xi-\xi_R(s,t)}{\Delta\xi(v;s,t)}\right)^2\right) + \exp\left(-\left(\frac{\xi+\xi_R(s,t)}{\Delta\xi(v;s,t)}\right)^2\right)\right] \ .$$

The dependencies of this Ansatz, via its exponent terms with $\xi - \xi_R$, are justified by assuming a 'rabbit ears' shape of the distribution function[29]. In particular, it is assumed that we have trapped ions with $\xi = \xi_R$, i.e. their turning points along the resonance layer where $v_\parallel$ is zero (and thus $\eta = 0$). The width of the distribution function, $\Delta\xi$, determines how strong this rabbit ear shape is.

These 'rabbit ears' shape of the distribution function during ICRH were also obtained, from simulations with bounce-averaged codes, in $(E, \eta = \frac{v_\parallel}{v_\perp})$ phase space coordinates. Thus, as the formerly computed $F(v; s, t)$ must be kept, and in order to mock up the 'rabbit ears' distribution, the following expression is proposed as approximation of $f_0(v, \xi; s, t)$:

$$f_0(v,\xi;s,t) = F(v;s,t)\mathcal{C}(v;s,t)\left[\exp\left(-\left(\frac{\xi-\xi_R(s,t)}{\Delta\xi(v;s,t)}\right)^2\right) + \exp\left(-\left(\frac{\xi+\xi_R(s,t)}{\Delta\xi(v;s,t)}\right)^2\right)\right] \ . \tag{3.2}$$

Essentially, F is extended to f_0 by introducing an Ansatz such that it follows the desired 'rabbit ears' shape, shown in Figure 4.1, and a certain normalization constant $\mathcal{C}$ so that f_0 is consistent with F.

Furthermore, the implicit dependency of f_0 on θ and η comes from the same implicit

dependence of ξ, from magnetic moment conservation. They can be related through (3.1) as

$$\xi(\eta,\theta;s,t)=\sqrt{1-(1-\eta^2)\frac{B_0(s;t)}{B(s,\theta;t)}}\ . \tag{3.3}$$

In this sense, f_0 depends on v,η,θ taking different values when given different parameters (s,t). Below $\xi_R,\Delta\xi,\mathcal{C}$ are reviewed and its calculation explained.

3.2.2 $\Delta\xi$ calculation

While ξ_R is defined as stated before and directly computed by $\xi_R(s,t):=\sqrt{1-\frac{B_0(s;t)}{B_0(s_R;t)}}$, where s_R represents the flux label corresponding to the resonance; the value of $\Delta\xi$ must be computed consistently with f_0 so that it meets its expected shape.

Namely, on the one hand, we assume $\Delta\xi$ is such that the averaged square of the cosine of the pitch angle η of a particle measured at the (poloidal) resonance position $\theta=\theta_R$, $\langle\eta_R^2\rangle$, can be properly computed by using (3.2) distribution function. That is, $\Delta\xi(v;s,t)$ is such that

$$\langle\eta_R^2\rangle(v;s,t)=\frac{\int\eta^2 f_0(v,\xi(\eta,\theta_R;s,t);s,t)d\eta}{\int f_0(v,\xi(\eta,\theta_R;s,t);s,t)d\eta}\ . \tag{3.4a}$$

On the other hand, as rough approximation, we use the model suggested by Anderson[14] to compute η in function of v (and s,t as parameters)

$$\left\langle\eta_R^2\right\rangle(v;s,t)=\frac{1}{3}\frac{1+\left(\frac{v}{v_*(s)}\right)^2}{1+\left(\frac{v}{v_*(s,t)}\right)^2+\left(\frac{v}{v_*(s,t)}\right)^4}\ . \tag{3.4b}$$

Where $v_*=\frac{v_\gamma(s,t)}{2}$ and v_γ is the characteristic velocity associated with pitch angle scattering[9]. This calculation of v_* works reasonably well in the limit $\frac{\mathrm{r}}{\mathrm{R}}\to 0$ (as happens in current tokamaks), but we assume it also works for finite r.

Therefore, and for each $(v;s,t)$, by equating (3.4a) and (3.4b) we can numerically retrieve the value of $\Delta\xi(v;s,t)$ such that fulfills the equations. This problem is amenable to numerical schemes such as Newton-Raphson's or the bisection method.

Notice that, although ξ_R is known, the value of $\mathcal{C}$ lacks for f_0 to be computed and, apparently, it would prevent carrying out the previous approach. However, since $\mathcal{C}$ does not depend on η, the fraction of (3.4a) cancels out this term.

3.2.3 $\mathcal{C}$ calculation

Similarly to how $\Delta\xi(v;s,t)$ is defined, and described in subsection 3.2.2, $\mathcal{C}(v;s,t)$ must also be computed so that f_0 is consistent with F. Namely, it is required that

$$F(v;s,t) \equiv \langle \hat{f}_0 \rangle (v;s,t) \ , \text{ where } \langle \hat{f}_0 \rangle (v;s,t) \coloneqq \int_{-\pi}^{\theta=\pi} d\theta \int_{-1}^{\eta=1} d\eta f_0(v, \xi(\eta,\theta;s,t);s,t) \ . \tag{3.5}$$

Here $\langle \hat{f}_0 \rangle (v;s,t)$ represents the pitch-angle **integrated** version of f_0, $\hat{f}_0$, when **integrated** along the poloidal surface, $\langle \hat{f}_0 \rangle (v;s,t)$.

Therefore, when $F(v;s,t) \neq 0$, $\mathcal{C}(v;s,t)$ must be such that

$$\mathcal{C}(v;s,t) \equiv \left[\int_{-\pi}^{\theta=\pi} d\theta \int_{-1}^{\eta=1} d\eta \exp\left(- \left(\frac{\xi(\eta,\theta;s,t) - \xi_R(s,t)}{\Delta\xi(v;s,t)} \right)^2 \right) + \exp\left(- \left(\frac{\xi(\eta,\theta;s,t) + \xi_R(s,t)}{\Delta\xi(v;s,t)} \right)^2 \right) \right]^{-1} \tag{3.6}$$

Note that, unlike the pitch-angle averaged $1D$ function $F(v;s,t)$, f_0 allows the definition of the poloidal resonant ion density $n_0(s,\theta;t)$ as

$$n_0(s,\theta;t) \coloneqq \int_{-1}^{\eta=1} d\eta \int_{0}^{v=+\infty} dv \ v^2 f_0(v, \xi(\eta,\theta;s,t);s,t) \ . \tag{3.7}$$

If (3.5) holds, then resonant ion densities $n(s;t)$ and $\langle n_0 \rangle (s;t)$, computed using F and f_0 respectively, are clearly identical since

$$\langle n_0 \rangle (s;t) \coloneqq \int_{-\pi}^{\theta=\pi} d\theta \ n_0(s,\theta;t) \ . \tag{3.8}$$

3.3 Numerical implementation

With the purpose of compute the $2D$ distribution function $f_0(v,\xi,s,t)$, as well as to visualize the results, some routines were created addressing the following points:

- To import all the needed experimental data and the PION data. For instance, on the one hand ξ_R was computed by definition $\xi_R(s,t) \coloneqq \sqrt{1 - \frac{B_0(s)}{B_0(s_R)}}$ using the toroidal magnetic field $B_0(s;t) \coloneqq B(s,0;t)$ from experimental data. On the other hand, $F(v;s,t)$ was imported from the PION data.
- To numerically solve $\Delta\xi$ (through bisection method) equating (3.4a) and (3.4b). The values of $v_*(s)$ were obtained as $v_*(s) = \frac{1}{2} v_\gamma$, being $v_\gamma = \sqrt{\frac{2E_{\text{crit}}}{m_e}}$ the characteristic velocity evaluated from the so-called critical energy[18], [19] E_{crit}.
- To numerically compute $\mathcal{C}$ as indicated by equation (3.6). The numerical integration was numerically carried out with a trapezoidal scheme, using the former values ξ_R and $\Delta\xi$.
- To numerically integrate f_0 in function of η, so that all identical ions but with different pitch angle compute equally for some representations, and leave it as a function of θ (and v,s,t).

- To visualize the flux surfaces for different s (Figure 1.1b).
- To visualize both the Ansatz and f_0 in (R, Z) plane (Figures 4.3, 4.4, 4.5), but also in (E, η) plane for the Ansatz (Figure 4.1).
- To visualize other quantities, such as ξ as function of θ (Figure 4.2).

Chapter 4

Numerical results

This chapter is devoted to review of the $2D$ distribution function f_0 proposed in terms of the obtained numerical results and plots.

In particular, a pure D plasma with 5% of hydrogen H minority is studied, modeling through f_0 the resonant ions of this hydrogen minority. Furthermore, the data used corresponds to the AUG experiment with '38017' as shot number, with 4 antennas emitting $36.5\ \mathrm{MHz}$ frequency waves and with an input power around $\sim 3.5\ \mathrm{MW}$, and a toroidal magnetic field B_ϕ whose values ranged from $\approx 1.90\ \mathrm{T}$ to $3.96\ \mathrm{T}$ depending on s, t, θ. The system will be **studied at the time slice** $t = 2.5\ \mathrm{s}$.

Specifically, the `PION` code was firstly run with the default ICRH settings, that is keeping the above frequency and power, and the plots associated to it are presented and discussed below. Afterwards, in sections 4.1 and 4.2, the power and frequency are respectively modified in order to compare the results with the expected outcome.

In order to treat PION data and to numerically expand $F(v; s, t)$ to the $2D$ distribution function $f_0(v, \xi, s, t)$, as well as to visualize the results, some Python codes were created and ran. More specifically, the developed routines addressed all the points listed at section **??**.

First of all, as validity check of the proposed 2D distribution, Figure 4.1 is presented. Furthermore, Figure 4.1 clearly displayed the desired feature of 'rabbit ears' shape that our $\mathrm{Ansatz}(\eta, \theta; s, t)$ must possess in (E, η) plane.

Note the closer to midplane $\theta = 0$, left subplot, the brighter and more separate these 'ears' are. Heuristically, this experimental phenomenon is well described by the proposed Ansatz because of the behavior of ξ, shown in Figure 4.2.

Specifically, comparing the abscissa $E = 500\ \mathrm{keV}$ of the left subplot of Figure 4.1 (associated to values $s = 0.25$ and $\theta = 0$, whence $\eta(\theta = 0) = \xi$), with the abscissa $\theta = 0$ of the middle subplot of Figure 4.2 (associated to $s = 0.3, E = 500\ \mathrm{keV}$); then we can explain the local maximums that 'rabbit ears present'. Namely, it is easy to observe that for such abscissas, when η is close to 0.2 then it cuts ξ_R. Thus, one of the Ansatz exponents cancels out, becoming $\mathrm{Ansatz}(v, \xi; s, t) = 1 + \exp\left(-\left(\frac{\xi+\xi_R}{\Delta\xi}\right)^2\right)$ a local maximum and, thus, appearing a 'rabbit ear' in $\eta \approx 0.2$. This is exactly what observed in Figure 4.1: for $E = 500\ \mathrm{keV}$ and $\theta = 0$ the brighter value of the Ansatz is for $\eta \approx 0.2$ (and analogously for its negative counterpart).

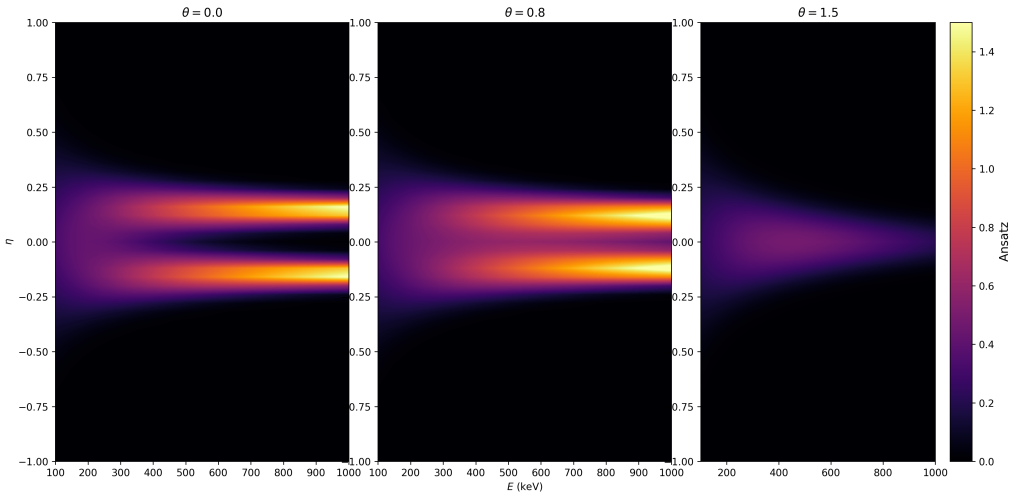

Figure 4.1: Plots of the Ansatz in the (η, E) space for different values of θ when (s, t) have fixed values of $(s, t) = (0.25, 2.5\ \mathrm{s})$. Note the mocked 'rabbit-ears' shape appears clearly, specially for 'central' values of θ.

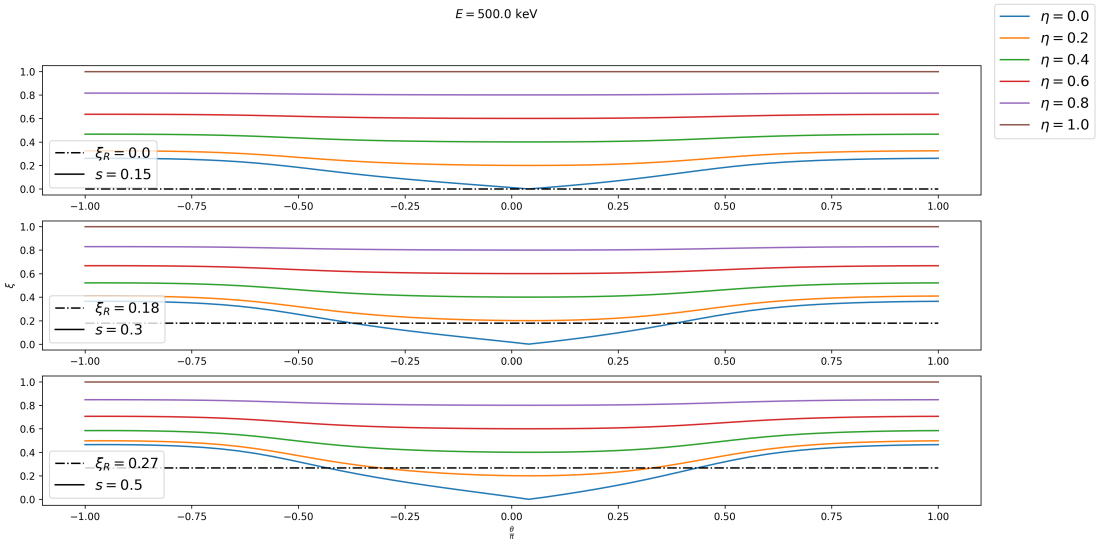

Figure 4.2: Plots of the midplane pitch-angle ξ as function of the poloidal angle θ (normalized with respect to π) for several values of s and fixed energy $E = 350\ \mathrm{keV}$. The dashed-dotted line represents the value of $\xi_R(s; t)$ (for $t = 2.5\ \mathrm{s}$ as the rest of cases).

On the other hand, even though is not shown in this work, f_0 was confirmed to be consistent with F. Specifically, the total minority density (3.8) was computed for different flux surfaces s and compared to the total ion density, which is correctly modeled with an error bar of 20%. Then, the ratio between them was around a 5%, the same result than using F to find this minority density ratio. Both results agrees with what is expected because the H ions constitute

around a 5% of the total ions in this shot to achieve minority heating (see 1.2.3).

Moreover, note that, since neither F nor $\mathcal{C}$ depends on θ, the variation on the poloidal angle of f_0 will be due to the $\mathrm{Ansatz}(v, \eta, \theta; s, t)$. In Figure 4.3, the $2D$ proposed distribution function f_0 is represented in (R, Z) coordinates to account for these differences, and it is displayed integrated along the pitch angle η. The integral on η is carried out so that ions with same energy but different velocity direction, and so pitch-angle, contribute equally to the representation.

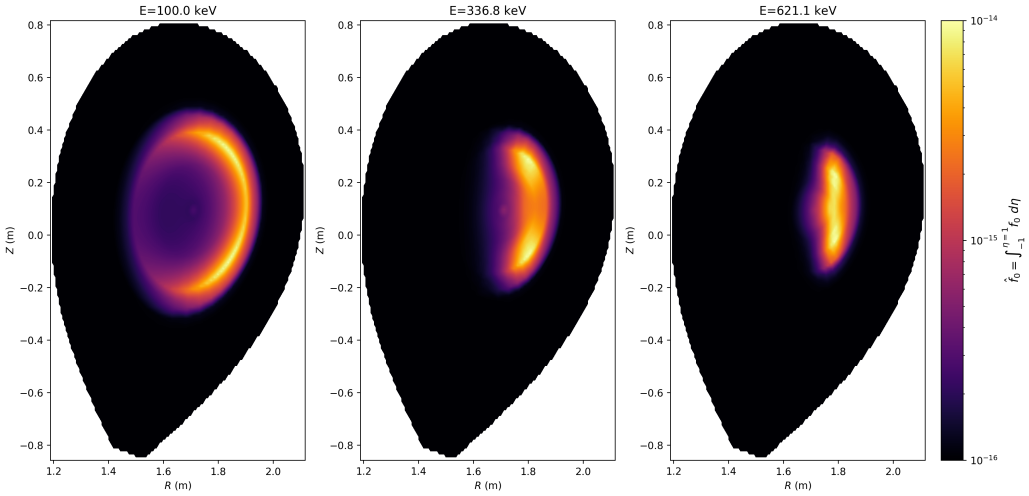

Figure 4.3: Plots of the $2D$ distribution function f_0, integrated along the pitch-angle η, in (R, Z) coordinates for different energies.

Let us note Figure 4.3 proves the heuristic intuition of what kind of distribution follow ICRH resonant ions: an almost homogeneous distribution of (thermal-energy) ions for low energy with an anisotropic tail for high energies. Moreover, the homogeneous contribution for low energies corresponding to a 'central spot' in purple, vanishes while energy increases (in the lowest energy $E = 100$ keV left subplot is clearly visible, whilst in the highest energy $E \approxeq 620$ keV right subplot is nonexistent).

We can also see that, the anisotropic distribution for high energies corresponds to a set of 'trapped particles' in the form of a 'banana orbit' in the low field side (for $R > R_0$, being R_0 the R coordinate at the center of the midplane). Yet, the more energetic ions are, then the more anisotropic their distribution is, for this 'banana orbit' becomes clearer and more narrow. For $E \approx 600$ keV, right subplot of Figure 4.3, the orbit of trapped ions resembles a vertical line which is centered at the so-called resonance position and whose flux surface is labeled by s_R. Moreover, the ions seem to gather specially at the tips of these 'banana' orbits, specifically while the energy is increased.

In view of the already great agreement of f_0, and in order to further check its validity, in subsections 4.1 and 4.2 the `PION` code is re-run with different input parameters.

4.1 Changing ICRH power

This section is devoted to the analysis of ICRH resonant ions distribution when the ICRH power has been modified. Specifically, while Figure 4.4a corresponds to the `PION` run with an increase of 300% of the section 4 ICRH power, Figure 4.4b is associated with a decrease until the 40% of the default setting.

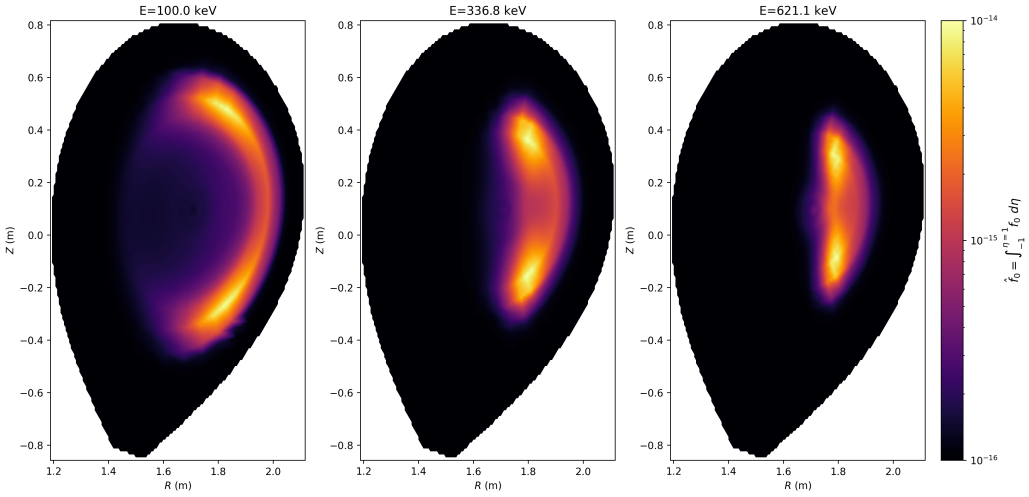

(a) 300%

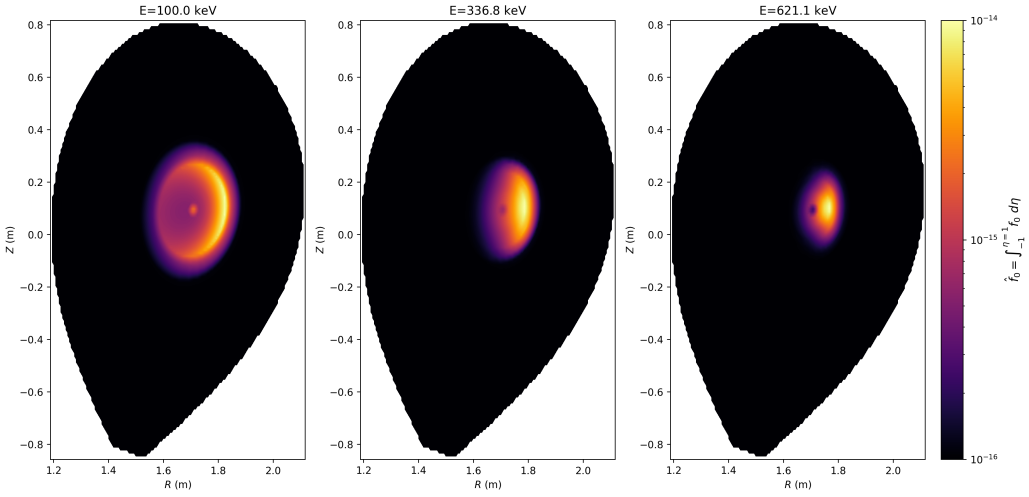

(b) 40%

Figure 4.4: Plots of the $2D$ distribution function f_0, integrated along the pitch-angle η, in (R, Z) coordinates for different power (the percentage compares the power value with the default one).

The effects of modifying ICRH power could be summarized as:

- ICRH with higher input power implies a higher average energy, as well as the fact more ions will be damped and become trapped, while it implies the contrary for lower power.
- Besides, the anisotropic effects of the high energy tail seem to be accentuated (dimmed) if the supplied power is increased (decreased). Actually, for same energy $E = 100\ \mathrm{keV}$, Figure 4.4b seems to resemble a thermal energy distribution that is much more homogeneous than 4.4a.

4.2 Changing ICRH resonance position

Similarly to section 4.2, this is devoted to the analysis of ICRH resonant ions when the resonance position is altered. In order to modify the resonance location, the wave frequency of the tokamak antennas must be changed.

The cyclotron frequency - or gyrofrequency - f is given by $f = \dfrac{q_i}{2\pi m_i} B$ where q_i, m_i are the charge and mass of the ion species i and B the toroidal magnetic field. Besides, the toroidal magnetic field in the midplane $B_0(s) = B(\theta = 0, s)$ verifies $B_0 \propto \frac{1}{R} \propto\!\!\!\sim \frac{1}{s}$ and, thus, it is held $f \propto B \propto B_0 \propto \frac{1}{R}$. Namely, an increase of frequency means the resonance is displaced to the 'left', that is, closer to the high field side HFS.

The effects of modifying ICRH frequency are shown through Figures 4.5a and 4.5b, in which frequency has been respectively set to $40\ \mathrm{MHz}$ and $33\ \mathrm{MHz}$ (in comparison to the $36.5\ \mathrm{MHz}$ of the default run). The consequences of these variations could be summarized as:

- ICRH with higher (lower) frequency implies a left (right) shift, towards the HFS (LFS), of the resonance position, as expected. However, it should be said the resonance position was expected to be more in the HFS than actually it is.
- While for higher frequency the anisotropic effects of the high energy tail seem to dim, they appear easier for lower frequency. Also, the width of this 'banana' shape orbit and the concentration of trapped ions in the tips of these orbits seem to increase.

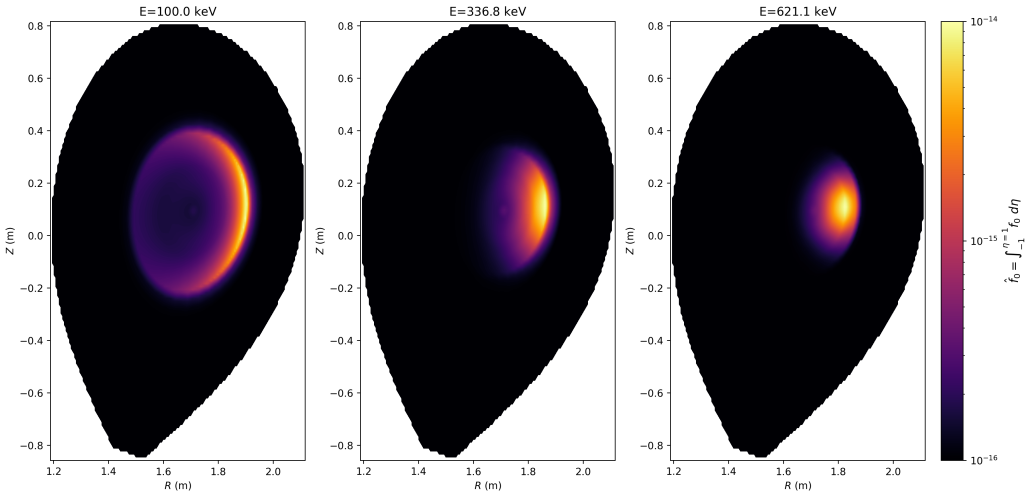

(a) $f = 40\text{MHz}$

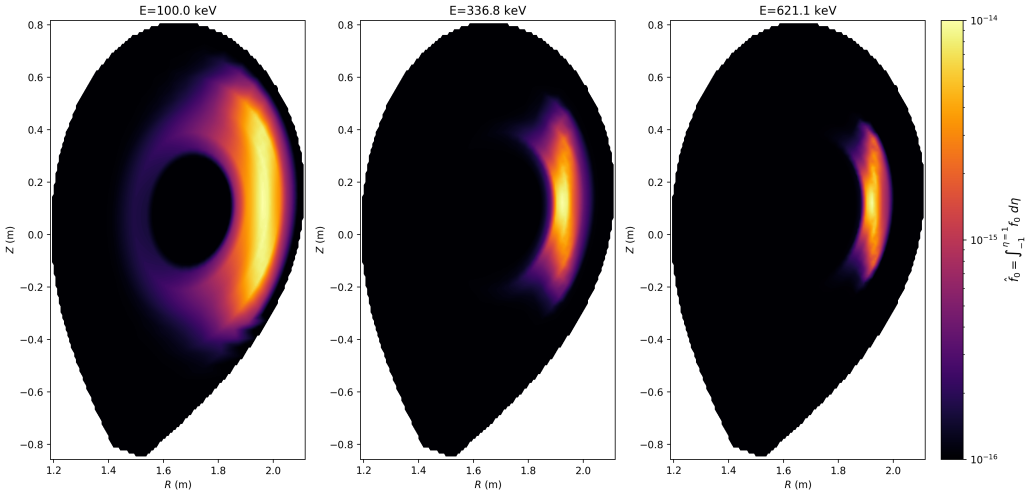

(b) $f = 33\text{MHz}$

Figure 4.5: Plots of the $2D$ distribution function f_0, integrated along the pitch-angle η, in (R, Z) coordinates for different energies when ICRH frequency is modified.

Chapter 5

Conclusions

Throughout this work, we have analytically and numerically studied fast ion populations during ICRH, specially emphasizing its description in terms of distribution function and, in particular, extending a $1D$ description $F(v;s,t)$ to a $2D$ description $f_0(v,\xi;s,t)$.

In particular, a first brief presentation of the basics of confined fusion and ICRH was given in chapter 1. Also, the role of ICRF waves to effectively raise plasma temperature was justified and its consequences on the ion distribution presented. Moreover, it was highlighted the necessity of introducing a minority concentration of hydrogen H in single ion species plasmas, as well as the importance of an accurate distribution function to describe these resonant ions.

Afterwards, a thorough review of the most common distribution functions for ICRH resonant ions was carried out in chapter 2. There, both the heuristic conception and the theoretical description of these ions were given. Specifically, it was seen ions qualitatively behave as Maxwellian (thermal-energy) particles for low velocities, but with a strongly anisotropic energy tail for high velocities and energies. Besides, it was also presented the $1D$ pitch-angle averaged distribution function F that is currently being used in the `PION` code.

Then, a $2D$ extension of the resonant ions distribution function f_0 was analytically reviewed in chapter 3.

At last, a numerical study was carried out in chapter 4 using experimental data from an AUG ICRH experiment and with numerical results from `PION`. The proposed $2D$ extension f_0 was initially tested applying $36.5\ \mathrm{MHz}$ and $\sim 3.5\ \mathrm{MW}$ ICRF waves to a pure D plasma with 5% H minority. Finally, the ICRF wave frequency and ICRF input power were varied to study the dependence of the resonant ions distribution on these key parameters.

The proposed distribution f_0 found good agreement with the expected results, and in particular, it was consistent with $1D$ function F. Thus, this suggested distribution is an effective means of adding a pitch (and poloidal) dependency to the current `PION` description of plasma resonant ions, improving its capabilities as it was desired.

This improvement is of interest since it will allow new comparisons with fast ion measurements with various diagnostics for further validations of the code against experimental data. Experimental validation is of vital importance to increase our confidence in our simulations of new experiments with ICRF heating both in present devices and future devices such as ITER.

Bibliography

[1] D. Gallart Escolà. *Computational analysis of ion cyclotron resonance frequency heating for JET experiments* Universitat Politècnica de Catalunya. Departament de Física, Spain (2019). http://hdl.handle.net/10803/669438

[2] S. Pfalzner. *An Introduction to Inertial Confinement Fusion.* Taylor and Francis Group, London (2006).

[3] L. Spitzer et al. *The Electrical Conductivity of an Ionized Gas*. Physical Review, 80 (2):230–238 (1950).

[4] F. Dini, R. Baghdadi, R. Amrollahi, S. Khorasani. *An overview of plasma confinement in toroidal systems.* Horizons in World Physics, p. 71-185. (2011).

[5] T.H. Stix et al. *Heating of toroidal plasmas by neutral injection*. Plasma Physics, 14:367 (1972).

[6] J. Freidberg. *Plasma Physics and Fusion Energy*. Cambridge University Press, New York (2007).

[7] J. Wesson. *Tokamaks*. Oxford Science Publications, Oxford (1997).

[8] L.-G. Eriksson, T. Hellsten, U. Willen. Nuclear Fusion, 33:1037. (1993)

[9] T. H. Stix. *Fast wave heating of a two component plasma*. Nuclear Fusion, 15:737. (1975).

[10] D. Anderson, W.G.F. Core, L-G. Eriksson, H. Hamnén, T. Hellsten and M. Lisak. *Distortion of ion velocity distributions in the presence of ICRH A semi-analytical analysis.* Nucl. Fusion 27, 911. (1986).

[11] S. Succi, K. Appert, W. Core, H. Hamnen, T. Hellsten and J. Vaclavik. *Computational Models for Wave-Particle Interaction, NUMOP (Numerical Modelling of Plasmas).* Varenna (1985) and Comp. Phys. Comm., 40, 137 (1986).

[12] D. J. Anderson Plasma Phys. 29, (1983) 317.

[13] D.J. Anderson, W.G.F. Core, L-G. Eriksson, H. Hamnén, T. Hellsten and M. Lisak. Nucl. Fusion 27, (1987) 911.

[14] D. Anderson et al.. Plasma Phys. Control. Fusion 29 (1987) 891.

[15] L.G. Eriksson et al. *Monte Carlo operators for orbit-averaged Fokker–Planck equations*. Physics of Plasmas, 1:308 (1994).

[16] A. N. Kaufman. Phys. Fluids 15, 1061. (1972). https://doi.org/10.1063/1.169403

[17] L.-G. Eriksson and P. Helander.. Phys. Plasmas 1, 308. (1994).

[18] M. J. Mantsinen. *Development and Experimental Evaluation of Theoretical Models for Ion Cyclotron Resonance Frequency Heating of Tokamak Plasmas*. PhD thesis, Helsinki University of Technology, Department of Engineering Physics and Mathematics, Espoo, Finland. (1999).

[19] M. J. Mantsinen. *Bulk Ion Heating with ICRF Waves in Tokamaks.* Radio Frequency Power in Plasmas, AIP Conf. Proceedings. 1689, 030005-1–030005-8. (2015) https://doi.org/10.1063/1.4936470

[20] J. Hedin *Ion Cyclotron Resonance Heating in Toroidal Plasmas.* PhD thesis, Alfvén Laboratory, Division of Fusion Plasma Physics. Royal Institute of Technology, Stockholm (2001).

[21] J. Carlsson. *Ion Cyclotron Resonace Heating and Current Drive in Tokamaks*. Ph.D. thesis, Royal Institute of Technology, ISBN 97-7107-237-7. (1998).

[22] J. Carlsson, T. Hellsten and L.-G. Eriksson. Technical Report ALF-1996-104, Alfvén Laboratory, Royal Institute of Technology, SE-100 44 STOCKHOLM, SWEDEN, (1996).

[23] T.H. Otway. *Mathematical Aspects of the Cold Plasma Model.* Perspectives in Mathematical Sciences, pp. 181-210 (2010) http://doi.org/10.1142/9789814289313_0009

[24] T. Hellsten et al. *Power deposition for ion cyclotron heating in large tokamaks.* Nuclear Fusion, $28 : 285, 1988$.

[25] L. Villard. *Global waves in cold plasmas.* Computer Physics Reports, $4 : 95, 1986$.

[26] X. Llobet et al. *Theory of Fusion Plasmas.* Editrice Compositori, Bologna, 1996 .

[27] T. Hellsten et al. *A modelling scheme for the direct electron heating profiles during ion cyclotron resonance heating.* Nuclear Fusion, $29 : 2165, 1989$.

[28] L.-G. Eriksson and T. Hellsten. *A Model for Calculating ICRH Power Deposition and Velocity Distribution.* Physica Scrypta, $55 : 70, 1995$.

[29] G.D. Kerbel, M.G. McCoy. *Kinetic theory and simulation of multispecies plasmas in tokamaks excited with electromagnetic waves in the ion-cyclotron range of frequencies*. The Physics of Fluids 28, 3629 (1985). https://doi.org/10.1063/1.865319.

[30] I.L. Arbina et al. *First applications of the ICRF modelling code PION in the ITER Integrated Modelling and Analysis Suite.* 46th EPS Conference on Plasma Physics. P4.1079. (2019)

[31] M. Mantsinen et al. *Analysis of bulk ion heating with ICRH in JET highperformance plasmas.* Plasma Physics and Controlled Fusion, 41:843, 1999.

[32] M.J. Mantsinen et al. *Third harmonic ICRF heating of deuterium beam ions on ASDEX Upgrade.* 43rd EPS Conference on Plasma Physics, 40A:030005, 2016.

[33] L.-G. Eriksson et al. *On the role of ion heating in ICRF heated discharges in Tore Supra.* Physics of Plasmas, 24:022122, 2017.

[34] M. J. Mantsinen et al. *Analysis of combined fast wave current drive and neutral beam injection in the DIII-D tokamak.* Physics of Plasmas, 9:1318, 2002.

[35] V. Bergeaud et al. *ITER relevant ICRF heating scenarios with large ion heating fraction.* Nuclear Fusion, 40:35, 2000.

[36] D. Gallart et al. *Modelling of ICRF heating in DEMO with special emphasis on bulk ion heating.* AIP Conference Proceedings, 1689:060004, 2015.

[37] F. Imbeaux et al. *Design and first applications of the ITER integrated modelling & analysis suite.* Nucl. Fusion 55 123006 (2015). https://doi.org/10.1088/0029-5515/55/12/123006

[38] Yau, Stephen S.-T. *Computation of Fökker-Planck Equation.* Quarterly of Applied Mathematics, vol. 62, no. 4, 2004, pp. 643–650. JSTOR, www.jstor.org/stable/43638649.

[39] M. Schneider et al. (2015) Nucl. Fusion. 55. 013003

[40] Ya. I. Kolesnichenko, M. Lisak, V. V, Lutsenko, F. Wising *Space and Velocity Distributions of Fast Ions in Magnetically Confined Plasmas*, Chalmers Tekniska Högskola. Institutionen för elektromagnetisk fältteori. CTH-IEFT/PP-1994-12. ISSN: 0281-1308. (1994)

Declaració d'Autoria del Treball de Fi de Grau

Jo, Gerard Castro Castillo, amb Document Nacional d'Identitat 47982218D, i estudiant del Grau en Física de la Universitat Autònoma de Barcelona, en relació amb la memòria del treball de final de grau presentada per la seva defensa i avaluació durant la convocatòria de Juliol del curs 2020-2021, declara que:

- El document presentat és original i ha estat realitzat per la seva persona.
- El treball s'ha dut a terme principalment amb l'objectiu d'avaluar l'assignatura de treball de grau en física en la UAB, i no s'ha presentat prèviament per ser qualificat en l'avaluació de cap altra assignatura ni en aquesta ni en cap altra universitat.
- En el cas de continguts de treballs publicats per terceres persones, l'autoria està clarament atribuida, citant les fonts degudament.
- En el casos en els quals el meu treball s'ha realitzat en col·laboració amb altres investigadors i/o estudiants, es declara amb exactitud quines contribucions es deriven del treball de tercers i quines es deriven de la meva contribució.
- A l'excepció del punts esmentats anteriorment, el treball presentat és de la meva autoria.

Signat:

Declaració d'Extensió del Treball de Fi de Grau

Jo, Gerard Castro Castillo, amb Document Nacional d'Identitat $47982218\mathrm{D}$, i estudiant del Grau en Física de la Universitat Autònoma de Barcelona, en relació amb la memòria del treball de final de grau presentada per la seva defensa i avaluació durant la convocatòria de Juliol del curs 2020-2021, declara que:

- El nombre total de paraules (segons el comptatge proposat[1]) incloses les seccions des de la introducció a les conclusions és de 7521 paraules.
- El nombre total d'equacions és de 25.
- El nombre total de figures és de 7.

En total el document comptabilitza: 7521 paraules $+ 25 \times 20$ paraules/equació $+ 7 \times 200$ paraules/figura $= 9421$, que compleix amb la normativa en ser inferior a 10000.

Signat:

[1]Utilitza l'eina de comptatge de paraules de Word. La versió Word 365, amb llicència de campus UAB, permet obrir arxius pdf. Per tal de fer el comptatge s'ha de seleccionar el text des de la introducció fins a les conclusions. Queden exclosos del comptatge: abstract, referències, annexos i qualsevol document que no formi part pròpiament del cos del treball.

Declaració de Supervisió del Treball de Fi de Grau

Aquest document té com a objectiu certificar que l'alumne Gerard Castro Castillo, amb DNI 47982218D, ha realitzat el seu treball titulat *Fast ion populations during ion cyclotron resonance frequency heating in tokamaks* sota la meva direcció, i el presentarà per tal de defensar l'assignatura Treball final de grau en el Grau de física.

L'alumne m'ha fet arribar el formulari word d'avaluació de l'activitat de l'alumne per part del director(*siusplau, feu-lo arribar omplert a* `tfg.fisica@uab.cat` *abans del lliurament de les memòries*).

Directora del treball
Prof. Dr. Mervi Mantsinen

Barcelona Supercomputing Centre (BSC)
Fusion Group

Signatura: